The Gas diffusion electrode setup as a testing platform for evaluating fuel cell catalysts: a comparative RDE-GDE study

Sven Nösberger[a+], Jia Du[a+], Jonathan Quinson[b], Etienne Berner[a], Alessandro Zana[a], Gustav K.H. Wiberg[a], Matthias Arenz[a] *

[a] Department of Chemistry, Biochemistry and Pharmaceutical Sciences, University of Bern, Freiestrasse 3, 3012 Bern, Switzerland

[b] Department of Chemistry, University of Copenhagen, Universitetsparken 5, 2100 Copenhagen Ø, Denmark

[+] Equally contributing first authors

* Corresponding author: matthias.arenz@unibe.ch

Abstract

Gas diffusion electrode (GDE) setups have been recently introduced as a new experimental approach to test the performance of fuel cell catalysts. As compared to the state-of-the-art in fundamental research, i.e., rotating disk electrode (RDE) measurements, GDE measurements offer several advantages. Most importantly mass transport limitations, inherent to RDE measurements are avoided. In a GDE setup the reactant, e.g., oxygen gas, is not dissolved into a liquid electrolyte but distributed through a gas diffusion layer (GDL), as it is actually the case in fuel cells. Consequently, much higher current densities can be achieved, and the catalysts can be studied in a wider and more relevant potential range. Furthermore, direct contact to a liquid electrolyte can be avoided and elevated temperatures can be employed in a straight-forward

manner. However, the use of GDE setups also comes with some challenges. The determined performance is not strictly related to the catalyst itself (intrinsic activity), but also to the quality of the catalyst film preparation. Therefore, it might be even more important than in RDE testing to develop standardized procedures to prepare catalysts inks and films that can be reproduced effortlessly in research laboratories for fundamental and applied experimentation. To develop such standardized testing protocols, we present a comparative RDE – GDE study, where we investigate several commercial standard Pt/C fuel cell catalysts with respect to the oxygen reduction reaction (ORR). The study highlights the strengths of the GDE approach as an intermediate "testing step" between RDE and membrane electrode assembly (MEA) tests when developing new fuel catalysts.

Key words: Gas diffusion electrode (GDE) setups; fuel cell catalysts; oxygen reduction reaction (ORR); rotating disk electrode (RDE) measurements

1 Introduction

To minimize the global impact of climate change on human civilization, human welfare, and biodiversity, it remains crucial to reduce mankind global greenhouse gas emissions. To fulfil social and economic transformations defined by the legally binding Paris Climate Agreement, such as lowering the net CO_2 emissions to zero by 2050 thereby limiting the pre-industrial global temperature rise to 1.5 °C, alternative energy sources need to be developed. [1][2]. So far however, there have been obstacles to their development. A promising system are fuel cells that efficiently convert chemical energy to electric energy by combining hydrogen and oxygen to form water. [3][4] Despite their potential advantages, many potential applications of fuel cells are still considered too expensive and not yet commercially viable.

A major factor that determines the costs of the fuel cell technology is the use of Pt in the fuel cell catalysts. Thus, the catalyst layers need to be improved in a way that they provide maximal power by minimal Pt content. Additional challenges are the scarcity of the active catalyst materials and the limited conversion efficiency (as compared to battery storage). [5] Developing new and improved ORR catalysts with lower platinum content that achieve higher power densities is therefore crucial. One major challenge thereby is the implementation of new catalysts established in fundamental research to applications in fuel cells. In fundamental research most fuel cell catalysts are investigated with a rotating disc electrode (RDE) setup. [6] However, due to the limited mass transport, inherent to RDE setups, the potential ranges at which the kinetics of an ORR catalyst can be investigated is narrow. This limits the transferability of results gained with an RDE setup towards an application in fuel cells. There is a lack of evidence that high performing fuel cell catalysts measured with the RDE setup can unfold their full potential in membrane electrode assemblies (MEAs) that constitute a fuel cell [7] [8] [9].

In order to facilitate the full exploitation of results and knowledge obtained mainly in RDE measurements conducted in fundamental research, new measurement setups with increased mass transport properties have been introduced [8], [10]–[16]. These setups allow to apply more realistic conditions in the catalyst testing and at the same time should be widely applicable in standard research laboratories. The gas diffusion electrode (GDE) approach fulfils these criteria. [15][17]–[19] However, one major challenge is to develop and standardize procedures for catalyst testing in GDE setups. In the presented study, we therefore compare the ORR performance of six different commercial Pt/C catalysts in a GDE setup. Standardized RDE measurements serve as benchmark. It is demonstrated that a GDE approach allows a straight-forward optimization of a

given catalyst film under conditions relevant for applications. On the other hand, GDE testing using standardized ink recipes might not uncover the full potential of a respective catalyst.

2 Experimental

2.1 Chemicals, Gases, and commercial catalyst samples

Ultrapure water (resistivity > 18.2MΩ·cm, total organic carbon [TOC] < 5 ppb) from a Milli-Q system (Millipore) was used for catalyst ink formulation, acid/base dilutions and the GDE cell cleaning. For the ink formulation and electrolyte preparation following chemicals were used: isopropanol (IPA, 99.7 + %, Alfa Aesar), 70% perchloric acid ($HClO_4$, Suprapur, Merck), potassium hydroxide hydrate ($KOH \cdot H_2O$, Suprapur, Merck), commercial Pt/C catalysts (19.4 wt. % TEC10E20A, 46.0 wt. % TEC10E50E and 50.6 wt. % TEC10E50E-HT, Tanaka kikinzoku kogyo, as well as HiSPEC 3000, HiSPEC 9100, and HiSPEC 13100, Alpha Aesar) and Nafion dispersion (D1021, 10 wt%, EW1100, Fuel Cell Store). A Nafion membrane (Nafion 117, 183 µm thick, Fuel Cell Store), a gas diffusion layer (GDL) with a microporous layer (MPL) (Freudenberg H23C8) and a GDL without an MPL (Freudenberg H23) were employed in the GDE cell measurements. Before use, the Nafion membrane was prepared and activated as follows: after punching several discs with 2 cm diameter from a Nafion sheet, the discs were treated for 30 min at 80 °C in 5 wt.% H_2O_2, followed by rinsing with Milli-Q water. Then, the membrane discs were treated for 30 min at 80 °C in Milli-Q water followed by rinsing with Milli-Q water. Finally, the membrane discs were treated for 30 min at 80 °C in 8 wt.% H_2SO_4, again followed by rinsing with Milli-Q water. All membranes were kept in a glass vial filled with Milli-Q water. For the electrochemical measurements the following gases from Air Liquide were used: Ar (99.999%), O_2 (99.999%) and CO (99.97%).

2.2 Small angle X-ray scattering (SAXS)

Small angle X-ray scattering (SAXS) measurements were conducted at the University of Copenhagen, Niels Bohr Institute, Denmark, using a SAXSLab instrument as previously reported. [19] The instrument is equipped with a 100XL + micro-focus sealed X-ray tube from Rigaku, producing a photon beam with a wavelength of 1.54 Å. A 2D 300 K Dectris Pilatus detector was used to record the scattering patterns. The sample powders were placed in-between mica windows in home-made cells. The two-dimensional scattering data were azimuthally averaged and normalized by the incident radiation intensity, the sample exposure time, and the transmission, and then corrected for the background (carbon materal without nanoparticles) and detector inhomogeneities using the SAXGUI reduction software. The resulting dataset is the radially averaged intensity $I(q)$ expressed as a function of the scattering vector $q = 4\pi \cdot \sin(\vartheta)/ \lambda$, where λ is the wavelength and 2ϑ is the scattering angle.

The data were fitted assuming a power law and polydisperse spheres. The background corrected scattering data were fitted using a power law to take into account the behaviour at low q value and a model of polydisperse spheres described by a volume-weighted log-normal distribution. Some data were best fitted by adding a second model of polydisperse spheres also described by a volume-weighted log-normal distribution.

The scattering data are fitted to the following general expression:

$$I(q) = A \cdot q^{-n} + C_1 \cdot \int P_{S1}(q, R)\, V_1(R)\, Dv_1(R) dR + C_2 \cdot \int P_{S2}(q, R)\, V_2(R)\, Dv_2(R) dR$$

where $A \cdot q^{-n}$ corresponds to the power law where A and n are free parameters; C_1 and C_2 are scaling constants, P_{S1} and P_{S2} the sphere form factors, V_1 and V_2 the particle volumes and Dv_1 and Dv_2 the log-normal size distribution.

The sphere form factor is given by

$$P_s(q,R) = (3\frac{\sin(qR) - qR.cos(qR)}{(qR)^3})^2$$

D_V was assumed to be a log-normal distribution:

$$D_V(R) = \frac{1}{R\sigma\sqrt{2\pi}} e^{-\left(\frac{\left[\ln\frac{R}{R_0}\right]^2}{2\sigma^2}\right)}$$

where σ is the variance and R_0 the geometric mean of the log-normal distribution (evaluated here in Å). The fitting was conducted with the home-written MATLAB code available on request. The free parameters in the model are A, n, R_1, R_2, σ_1, σ_2, C_1, C_2. The scattering data and related fits are reported in Figure S 1 and the values obtained for the fitting parameters are reported in Table S 1.

2.3 Transmission electron microscopy (TEM) and scanning electron microscopy with energy dispersive X-ray spectroscopy (SEM-EDS)

A Jeol 2100 transmission electron microscope (TEM) operated at 200 kV was used for the TEM analysis. The samples were prepared by suspending the commercial catalyst powders in ethanol and then dropping the sample suspension onto carbon coated copper TEM grids (Copper or Nickel grids, Quantifoil). Micrographs were recorded in at three different magnifications at least, and in at least three randomly selected areas. At least 200 nanoparticle diameters were evaluated using the software ImageJ to evaluate the size distribution.

The SEM-EDS cross-section measurements were performed as described before [18] using a Zeiss GeminiSEM 450 with SmartSEM 6.05 software and EDS Photodetector Ultim max 65 from Oxford instruments using AZTec 4.2 software. As scan parameters for the EDS maps a WD (working distance) between 8.4 and 8.8 mm, accelerating voltage of 15 kV and a probe current of 200 pA were used.

2.4 Electrochemical characterization

2.4.1 Catalyst *ink and film formation for the RDE measurements*

The inks for the RDE measurements were prepared from the respective dried catalyst powder and dispersed in a mixture of Milli-Q water and isopropanol (V_{water}: V_{IPA}= 3: 1). To the ink 1.6 µL/ml 1 M KOH (aq) was added and then homogenized in a sonicator bath for 10 min. The resulting homogeneous catalyst ink had a total Pt concentration of 0.218 g_{Pt} L^{-1}.

Thin catalysts films were prepared by pipetting 9 µL (0.218 g_{Pt} L^{-1}) of each catalyst ink onto a newly polished glassy carbon (GC) disc. The disc was then dried in an argon atmosphere. The resulting films had a Pt loading of 10 µg cm^{-2} and were dried at ambient atmosphere for further electrochemical measurements.

2.4.2 Catalyst ink and film preparation for the GDE measurements

Catalysts inks were prepared from different dried catalyst powders and dispersed in a mixture of Milli-Q water and isopropanol (mixture volume ratio of 3:1). To disperse the powder, the mixture was sonicated for 5min at room temperature. Subsequently, Nafion solution was added so that the ink contained a mass C:Nafion ratio of 1. The ink was sonicated again for 5min. The final inks had a Pt concentration of 0.5 mg/ml for all catalysts.

The catalyst films were produced by a vacuum filtration of the catalyst ink onto GDL. To conduct the vacuum filtration, the ink was first diluted by Milli-Q water to a Pt concentration of 0.05 mg/ml. The ink was then added to a vacuum apparatus and filtrated through an MPL-coated GDL (Freudenberg H23C8). The resulting catalyst films (Ø =4cm) were stored in petri dishes. From this film coated GDL, a disk (Ø = 3mm) was extruded and used as GDE. All investigated GDEs prepared from the commercially available Pt/C catalysts had a Pt loading of 208 $ug_{Pt} \cdot cm^{-2}$ on the GDL.

2.4.3 Rotating disk electrode (RDE) measurements

All RDE electrochemical measurements were performed at room temperature with a computer controlled potentiostat (ECi 200, Nordic Electrochemistry ApS) and a glass cell equipped with 3 electrodes as previously reported.[20][21][22] The working electrode (WE) was a glassy carbon (GC) disk (5 mm in diameter) embedded into a Teflon tip.

A Pt wire served as counter electrode (CE) and a reversible hydrogen electrode (RHE) served as a reference electrode. An aqueous 0.1 M perchloric acid electrolyte was used which was saturated with argon prior to the start of the electrochemical measurements. The solution resistance was measured with a superposed AC signal (5mV, 5kHz) and was compensated down to 2 Ω.

The analytical procedure to electrochemically analyse the Pt/C catalyst layers was repeated for all six investigated Pt/C catalysts and included the following steps: Surface cleaning, Ar background, ORR activity, and CO stripping to determine Pt active surface area. The Pt catalyst surface was cleaned under an argon atmosphere by cycling the potential between 0.05 V_{RHE} and 1.20 V_{RHE} with a scan rate of 0.50 V s^{-1}. After roughly 50 cycles a stable cyclic voltammogram (CV) was observed. Afterwards, an Ar background was measured in a potential range between 0.05

V_{RHE} and 1.10 V_{RHE} with a scan rate of 0.05 V s^{-1} in Ar saturated electrolyte. Prior to the ORR performance measurements, the electrolyte was purged with O_2 for 10 min. During the ORR activity measurement, the potential window and the scan rate were the same as that applied for Ar background measurements, while the RDE had a rotation speed of 1600 rpm.

To determine the electrochemical active surface area (ECSA) of the investigated catalysts, the oxidation charge obtained from a CO monolayer stripping experiments was analysed. In brief, the electrode was held at 0.05 V_{RHE} in CO saturated electrolyte for 2 min. Subsequently, the electrolyte was saturated with Ar (~10 min) to purge the electrolyte from CO. The potential was swept from 0.05 to 1.10 V_{RHE} with a scan rate of 50 mV s^{-1} to oxidize the adsorbed CO monolayer to CO_2. The ECSA was then calculated from the ration of resulting oxidative charge (Q_{CO}), after background subtraction, and the oxidation charge of a monolayer, 400 µC cm_{Pt}^{-2}, and finally normalized to the mass of the Pt (m_{Pt}). [23]

$$ECSA = \frac{Q_{CO}}{400\mu C\ cm_{Pt}^{-2}} \frac{1}{m_{Pt}}$$

The ORR data was analysed from the background corrected polarization curves. The background polarization curves were recorded in Ar-purged electrolyte. The ORR activity was then evaluated at 0.90 V_{RHE} from positive going scans. The mass activity (MA) was obtained by normalizing the activity by the Pt mass. The specific activity (SA) was obtained by normalizing the measured current density (mA cm_{Geo}^{-2}) to the ECSA.

2.4.4 Measurements in the Gas Diffusion Electrode Setup

The GDE-setup was assembled as the follows [10]: A 3 mm disc was punched out of the catalyst film covered GDL. The catalyst containing disc was placed into an MPL-coated GDL disc (Ø = 2cm, Freudenberg H23C8) which had a 3mm hole in the middle. A Nafion membrane was placed on top (Nafion 117, thickness 183um). With a tablet press (pressure range: 0-15T), the whole stack was pressed together at a pressure of two tonnes and a duration of 10 min. Afterwards, a GDL (Freudenberg H23) was placed into the gas flow field of the lower cell body, followed by the stack containing the GDE and the Nafion membrane. Finally, the upper cell body was placed on top of the Nafion membrane. The two body parts were held in place by a clamp. The compartments of the upper cell body were filled with 15 ml of 4 M perchloric acid. Finally, an RHE and the CE (Pt wire) where put into the electrolyte.

All electrochemical measurements were performed at 30°C with a computer controlled potentiostat (ECi 240, Nordic Electrochemistry ApS) and a GDE-setup as reported. [10] The analytical procedure to electrochemically analyse the Pt/C catalyst layers was the same for all six investigated Pt/C catalysts and included the following steps: First, the GDE was purged from the backside (through the GDL) with argon gas. Doing so, the catalyst was cleaned by potential cycles between 0.05 and 1.10 V_{RHE} at a scan rate of 0.2 V s^{-1} until a stable cyclic voltammogram (CV) could be observed (~50 cycles). Afterwards, a CO-stripping measurement was performed followed by electrochemical impedance spectroscopy (EIS) and ORR-activity measurements. To conclude the investigations, a second CO-stripping measurement was performed. Throughout the entire experiment, a bubbler was used to humidify the gas and the membrane.

CO-stripping measurements were conducted to determine the ECSA. In essence, the catalyst layer got covered by CO gas which adsorbed onto the Pt surface. Afterwards, the catalyst was purged with Ar to remove the excess of CO. As a next step, a CV was recorded (scan rate 50 mV/s), which records the oxidative current originating from the oxidation of CO to CO_2. Finally, multiple CVs under Ar atmosphere were conducted until the Ar background was re-gained. The value of the ECSA was then obtained as previously described in section "2.4.3 Rotating disk electrode (RDE) measurements".

Prior to the ORR activity measurements, oxygen was flowed through the pipes for 10 minutes. For the last 5 minutes, a potential of 0.80 V_{RHE} was applied. This ensured that all gas lines were fully filled with oxygen and that the catalyst layer was equally wet over the entire surface. The ORR-activity measurements were conducted in potential control mode with a potential range between 1.00 V_{RHE} and 0.10 V_{RHE}. The potential was pre-set to 1.00 V_{RHE} and then lowered in steps of 25 mV until 0.10V_{RHE} are reached. At every step the potential was held constant for 1 minute to reach steady state conditions. For analysis, the measured current was averaged over the last 10 s. The solution resistance was measured by superposing a signal with a fixed frequency of 5kHz and an amplitude of 5mV. Finally, all ORR activity measurements were post-corrected for the potential errors introduced by the solution resistance.

3 Results and Discussion

3.1 Physical Characterization of the commercial Pt/C catalysts by TEM and SAXS

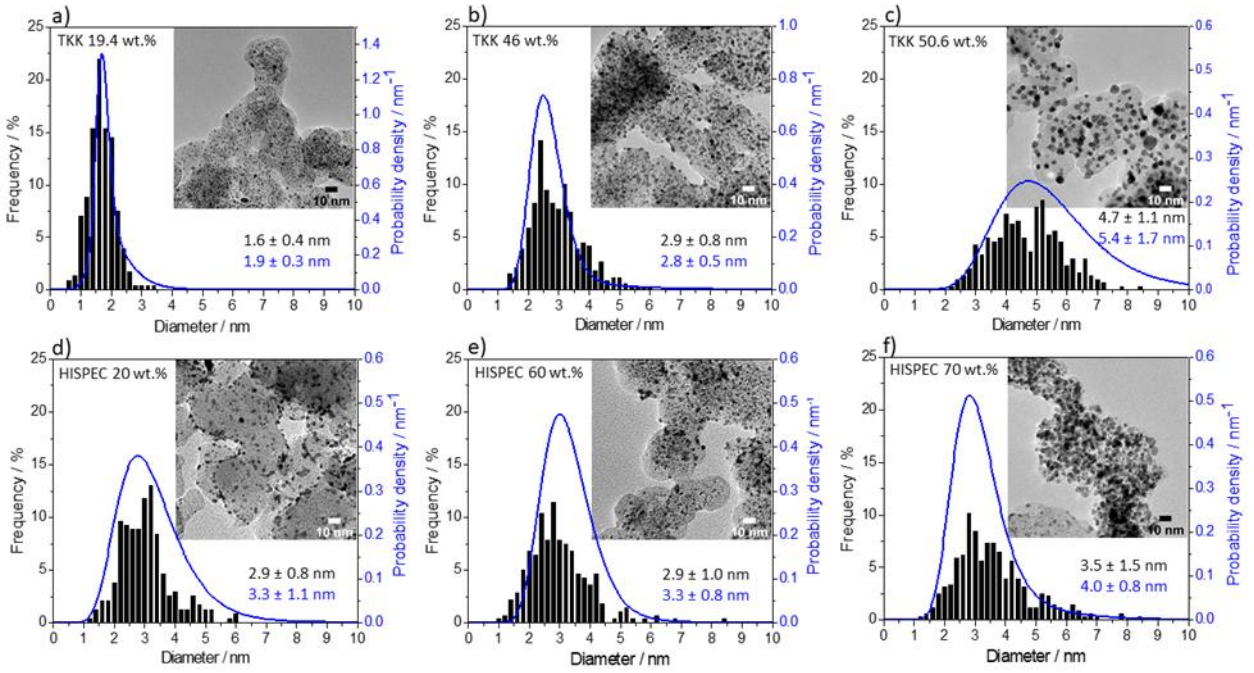

Figure 1: Pt particle size distribution of the investigated commercial Pt/C determined from TEM micrographs (at least 200 particles were counted) and probability density function derived from the SAXS analysis. The insets display representative TEM micrographs of each commercial Pt/C catalyst. The average particle size with the font in black is determined from TEM measurements while the blue font indicates the average particle size determined from the SAXS measurements. The Pt-to-C ratio (Pt loading) of each Pt/C catalyst is indicated in the upper left corner.

We start with the physical characterization of the investigated Pt/C fuel cell catalysts. All examined catalysts are commercially available and can serve as benchmarks in studies investigating new, home-made fuel cell catalysts. Their Pt to C ratio (Pt loading), as indicated by the supplier, ranges from roughly 20 wt. % up to 70 wt. %. In Figure 1, we present representative TEM micrographs to demonstrate the physical characteristics of each Pt/C catalyst. In addition, size histograms and average particle sizes derived from a TEM analysis as well as probability density functions derived from fitting the SAXS data are shown. As Figure 1 shows, within the accuracy (error) of the measurements both methods lead to the same average particle size.

However, with a closer look at the size retrieved, the average Pt particle size determined from TEM is slightly smaller (except for TKK 46 wt.% Pt/C) in comparison to the values derived from the SAXS analysis. This difference can be explained by the fact that the particle size distributions are based on different analyses that are sensitive to different sizes in different ways: For the TEM analysis, one determines the relative number of particles with the same size based on defined bin sizes and only relatively few individuals NP are accounted for. In contrast, SAXS analysis is performed in a larger volume of sample and so more NP are considered for the size evaluation. Additionally, the size retrieved from TEM is often number- or surface- weighted, whereas it is volume weighted for SAXS: i.e., SAXS is more sensitive to the contribution of larger NP sizes. This explains why SAXS analysis led to an estimated diameter slightly larger than for TEM analysis in this study. Nevertheless, due to the good agreement of the results obtained by both analysis techniques in the present study, we do not distinguish in the following between the two methods when referring to the average particle size and size distribution.

The analysis shows that the average particle sizes range from roughly 2 to 5 nm (Figure 1). In addition, the carbon support of each investigated catalyst is relatively homogeneously decorated by Pt particles; in particular the TKK 19.4 wt. % Pt/C sample. The limited particle agglomeration on the carbon support of this catalysts is also reflected by the very narrow size distribution with a standard deviation of only 0.4 nm in the TEM analysis. As expected, it can be clearly seen that at increased Pt loadings the carbon support is more densely covered with Pt particles and agglomeration increases. Characteristically in the TEM micrographs of the HISPEC 60 wt.% and 70 wt.% Pt/C samples, some darker spots are seen that most likely are related to the slightly

agglomerated Pt particles and the size distribution exhibits a clearly discernable tail towards larger sizes (also the size distribution of the TKK 50.6 wt. % Pt/C sample displays such a feature).

3.2 Physical Characterization of the as prepared GDEs from commercial Pt/C catalysts

In Figure 2, SEM-EDS cross sections of pristine GDEs prepared from three representative Pt/C catalysts are shown. The general structure of the GDEs consisting of a porous GDL covered by a carbon MPL and the respective Pt/C catalyst layer is clearly discernable. While the MPL's thickness is measured constantly to be around 20 µm, the thickness of the Pt/C catalyst layer varies with the Pt loading on the carbon support (Pt to carbon ratio) of the respective catalyst. At low Pt loading (20 wt. %) the catalyst film is about 16 ± 1 µm, whereas it is less than 5 µm on average at very high Pt loading (70 wt. %). In other words, higher Pt loadings (Pt to carbon ratio) of the Pt/C catalyst led to substantially denser (thinner) catalyst layers. Furthermore, the SEM micrographs imply that the vacuum filtration method of the Pt/C catalysts with high Pt loading leads to less homogeneous catalyst films on the GDL.

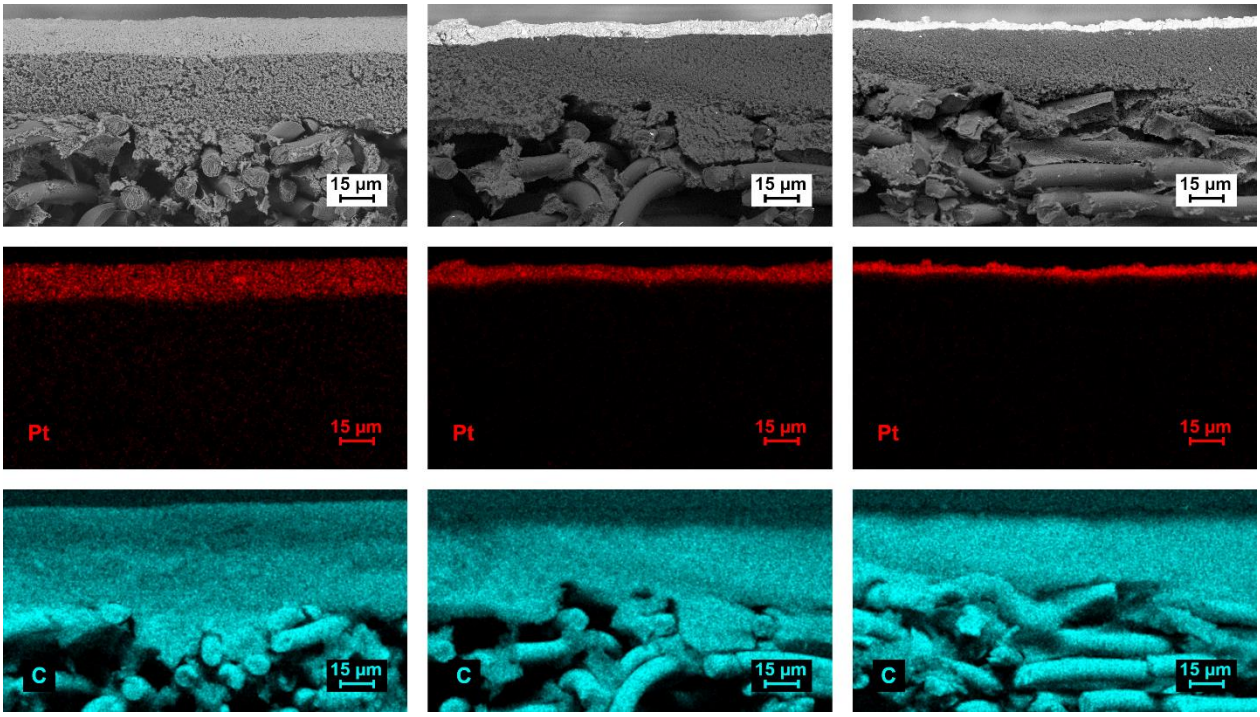

Figure 2: Comparison of SEM-EDS cross-sections of three GDEs prepared with different Pt/C catalysts. Left) HISPEC 20wt.%, middle) TKK 46wt.% and right) HISPEC 70wt.%. The SEM micrographs were recorded with the BSE detector. Due to the different metal loading on the carbon support in the Pt/C catalysts, the fixed Pt loading on the GDL (208 $ug_{Pt}cm^{-2}$) leads to different thicknesses of the catalyst film.

3.3 Electrochemical Catalyst Characterization: RDE vs. GDE

As mentioned in the introduction, one of the main motivations for introducing new measurement setups with increased mass transport has been the challenging implementation of promising catalysts identified in RDE measurements to fuel cells. Often the performance measured in a RDE setup cannot be translated to corresponding improvements in MEA measurements and there is a large gap between fundamental research and applications.[9] Therefore, it is of interest to systematically compare the performance of the Pt/C catalysts as determined by RDE measurements with their performance in GDE measurements. In previous work of our and other groups, the TKK 46 wt. % Pt/C sample was used as a benchmark or reference catalyst [10]–[14]. Therefore, in the following we discuss the GDE setup with this catalyst.

In Figure 3a representative CVs of the TKK 46 wt.% Pt/C samples recorded in the two setups are compared. In both cases, the typical “electrochemical features” of a Pt/C catalyst are depicted. In the low potential region of the CVs (0.05 - 0.35 V_{RHE}), both hydrogen adsorption (negative scanning direction) and desorption (positive scanning direction) are visible, typically referred to as H_{upd} peaks. However, the H_{upd} peaks in the CV of the GDE measurements slightly differ from the ones in the RDE, which are typical for measurements in aqueous perchloric acid electrolyte. In particular, in the CV recorded in the GDE setup the “second” peak at around 0.25 V_{RHE} is less pronounced, and the hydrogen evolution reaction (HER) starts earlier, around 0.07 V_{RHE}. In contrast to these differences, the adjacent potential region between 0.35 V_{RHE} and 0.60 V_{RHE}, the double layer region defined by capacitive currents from charging and discharging the interphase, displays identical double layer capacities in both setups. Finally, in the potential region of Pt oxidation and reduction (0.60 - 1.10 V_{RHE}), the Pt oxidation and reduction peaks in the CV recorded with the GDE setup are slightly shifted towards higher potentials. These observed differences are most likely a consequence of the different local ion environments. It is well-known that the hydrogen features are sensitive to the local ion-population. In the GDE setup the catalyst is surrounded by a solid Nafion electrolyte, whereas it is surrounded by a liquid aqueous electrolyte in the RDE setup. The earlier onset of the HER in the GDE setup might be related to the reduced local partial pressure of hydrogen.

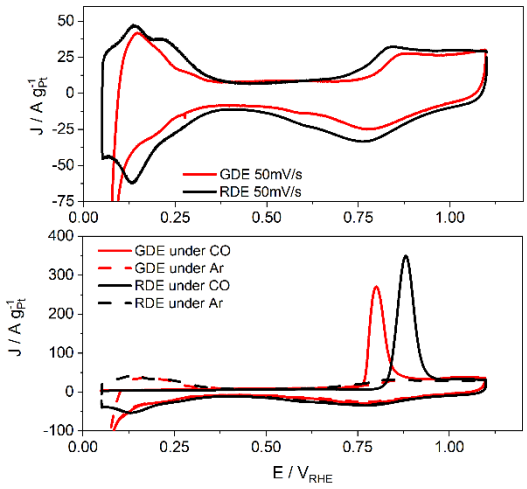

Figure 3: In the upper graph, representative examples of CVs of the same TKK 46 wt.% Pt/C catalyst recorded in an inert (Ar purging) atmosphere are shown, whereas in the lower graph, representative CO-stripping measurements of the same catalyst are shown. In red and black, we compare the normalized currents obtained from GDE and RDE. The CVs are normalized to the Pt loading on the electrode to take account of the different films thicknesses. The measurements recorded in the RDE setup are represented by a black line, while the measurements recorded in the GDE setup are represented by a red line. The scan rate amounts 50 mV/s for both GDE and RDE.

The effect of different reaction environment manifests itself even more in the CO stripping measurements that are typically used to determine the electrochemically active Pt surface area [24], see lower graph in Figure 3. The CO oxidation peaks recorded in both setups are clearly shifted against each other. Interestingly, in the GDE setup the CO stripping peak appears at lower potentials than in the RDE setup (ca. 0.8 vs. 0.9 V_{RHE}). Thus, the shift is more pronounced and in opposite direction as compared to the potential difference in oxide formation observed in the CVs recorded in Ar atmosphere. It should be pointed out that this shift is not related to an incomplete CO monolayer formation as can be seen from the absence of H_{upd} features in the forward going CO stripping scan. Furthermore, the H_{upd} peaks in the CV recorded after the CO stripping indicate that the surface area in both environments is very similar, see also below. Therefore it can be argued that the shift in the CO stripping peak is related to a reduced anion

blocking in the GDE membrane-catalyst environment [25]. Interestingly, the peak position observed in the CO stripping curve recorded in the GDE setup is similar to the one observed in an MEA measurement by Harzer et al. [26], although it needs to be stressed out that a direct comparison is difficult due to the different catalyst and different experimental parameters such as scan rate and temperature.

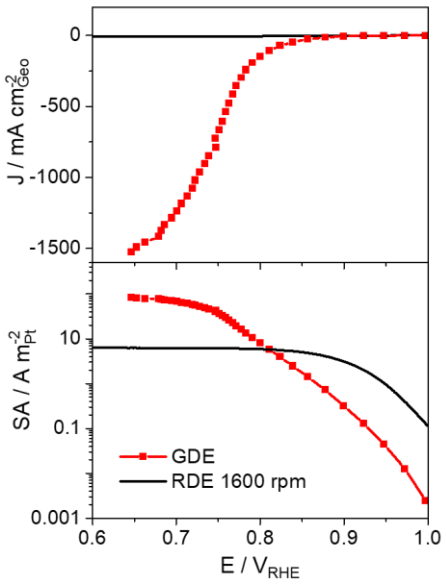

Figure 4: Comparison of the ORR performance of TKK 46 wt.% Pt/C measured in a GDE (red) and RDE setup (black). Upper graph, excerpt of the geometric ORR current densities. The adopted rpm rates for mass transport free extraction from RDE are 816, 1111, 1600, 2500 rpms, respectively.

In Figure 4, the behavior of the Pt/C benchmark catalyst in O_2 saturated atmosphere is presented from measurements by both setups, i.e., the RDE and the GDE setup. Focusing first on the measurement limitations of the RDE setup, it is demonstrated that the maximum ORR current density which can be reached (at 1600 rpm) is around 6 mA $cm^{-2}_{Geo.}$ The broad current plateau indicates that in a wide potential region the ORR is limited by mass transport through the hydrodynamic layer at the electrode interface. [27] By contrast, in the GDE setup a current density

up to 1400 mA cm^{-2}_{Geo} can be reached in the same potential region because oxygen gas can directly diffuse through the GDL to the catalyst layer. A GDE setup is thus particularly apt at investigating catalysts with higher current densities and lower potentials, which reflect more realistic conditions that are closer to the operational window for a real fuel cell. It should be mentioned though, that the maximum current density reached in the GDE setup can vary up to 50 % between different samples, highlighting the influence of the catalyst layer on the obtained results.

To further compare the results, the geometric current densities were normalized to the ECSA derived from the CO stripping measurements. The SA is shown in a Tafel plot, i.e. a logarithmic y-axis, in Figure 4's lower part. From this plot, the broader kinetic (linear) region can be observed, that goes from 1 V_{RHE} down to 0.75 V_{RHE} form GDE data. In contrast, for the RDE data, the linear region ends at around 0.90 V_{RHE}, due to the onset of diffusion limitations.

Astonishingly, the SA obtained in low-current regions (above 0.80 V_{RHE}) from RDE setup is significantly higher than the one measured in a GDE setup. This is caused by the fact that for GDE measurements we started at 1.00 V_{RHE} and went stepwise more negative to 0.10 V_{RHE}, where each step took 1 min. Thus, during the first few steps the catalyst had a steady state coverage of oxygenated species which partially block active sites. In contrast, dynamic potential cycling is used for RDE measurements. Here, the steady state coverage has not yet been obtained, and thus leads to an apparent higher activity. This is well-known from the different activities recorded in an RDE for the positive and negative going sweeps, respectively. [28] Both measurements protocols are typically used for respective setup, and thus, can lead to the appearance of different SA. To

support this statement, we performed a potential holding experiment in an RDE setup. (Figure S 3).

However, a GDE setup is not particularly designed to investigate the catalysts properties at 0.90 V_{RHE}, instead the focus is set to lower voltages with higher current densities, which reflects more realistic conditions, i.e., in the range between 0.70 V_{RHE} and 0.80 V_{RHE}. This range equals the operational window for a real fuel cell and is thus especially important. The kinetic region with the traditionally applied RDE setup is, however, not lower than 0.85 V_{RHE} (at around 0.85 V_{RHE} or below, the diffusion limited region is already reached due to reactant transport limitation), in comparison, the kinetic region from a GDE setup can be extended to 0.75V_{RHE}. Hence, a loss in activity at low current region in GDE is not decisive as a loss in high current regions.

3.4 Characterization and Comparison of different commercial Pt/C catalysts

In the following, the performance of the different commercial Pt/C catalysts in both setups is compared based on key values to highlight general trends.

3.4.1 ECSA

In Figure 5 the ECSA values of the different Pt/C catalysts measured in both setups is plotted vs. their “theoretical” ECSA, which is calculated from the TEM size histograms assuming that the Pt NPs are perfect, free-standing spheres, i.e., no Pt surface area is blocked by the carbon support. Part of the Pt/C samples can also be compared to previous measurements. [29] The diagonal line in Figure 5 indicates where measured and “theoretical” ECSA values are equal. It is demonstrated that there is in general a good agreement between the measured ECSAs and the expected ECSA based on the particle size distribution. However, the ECSA values determined in the GDE setup

are slightly lower than the ones obtained in the RDE measurements. This general trend is visualized in Figure 5 by fitting linear trendlines to the data points. The difference most likely is related to the presence of Nafion in the GDE catalyst layer. Nafion is known to partially block the active surface area of the active catalyst phase and thus reduces the ECSA [30]. By comparison, in the RDE measurements no Nafion binder was used.

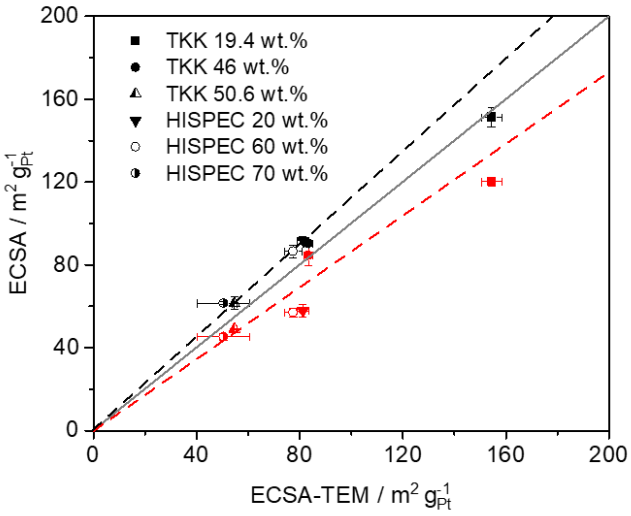

Figure 5: Comparison of ECSA values obtained from RDE (black dots) and GDE (red dots) measurements with the ECSA calculated from the Pt particle distribution shown in the TEM micrographs, indicated as ECSA-TEM. The ECSA-TEM values were calculated based on 200-400 randomly distributed Pt particles in the TEM micrographs of each catalyst. The given error with respect to the ECSA-TEM is the standard error of the counted Pt particles in TEM micrographs, while the given error from measured ECSA values is the standard deviation of at least three independent measurements of each catalyst.

3.4.2 ORR performance

The goal of an RDE characterization is to determine the intrinsic kinetic ORR activity of a catalyst. Such task is challenging as in the past even the results of relatively "simple" Pt/C catalysts had been varying by one order of magnitude [31]. As a result, benchmarks such as polycrystalline Pt have been introduced and several works on measurement procedures and best practices have been published [6], [20], [23], [24], [32], [33]. The basic assumption is that procedures and

conditions can be defined where all catalysts exhibit their maximum performance. Implementing such approach to GDE measurements we adopted a procedure of Yarlagadda et al. [34] to prepare Pt/C films on top of a GDL using the same Pt loading and a standardized ink composition for all Pt/C catalysts. Furthermore, the same automized testing protocol has been applied, see experimental section. The activity results then can be compared at either a fixed potential or at fixed current density. In the following, the performance of the different Pt/C catalysts is compared at a fixed current density of 5 A m_{Pt}^{-2}.

As Figure 4 shows, at low overpotentials the SA measured in a GDE setup is significantly lower than the one measured in an RDE setup. This loss in SA was observed for all six investigated Pt/C catalysts and is summarized in Figure 6. Figure 6 shows that with the used standardized procedure a potential shift in the range of 0.067 V_{RHE} and 0.108 V_{RHE} is observed between the two approaches which constitutes a substantial difference. These differences in performance can be attributed to several reasons. On the one hand, it needs to be noticed that RDE and GDE measurements are conducted using different procedures. RDE measurements are typically conducted potentiodynamically and only the forward-going, more active potential scan is analyzed at a fixed potential of 0.9 V_{RHE} as shown above in Figure 4. The obtained kinetic current density (after correcting for mass transport limitations) is considered as the intrinsic ORR activity of the catalyst surface. [35] However, the scan rate dependence [31] of such measurements clearly indicates that the ORR performance under such conditions might be overestimated. By comparison, the high current densities obtained in an GDE setup make such procedure difficult. Any uncompensated resistance (iR drop) leads not only to a shift in potential but also to a current dependent change in the scan rate. Potentiostatic or galvanostatic measurements by comparison

can be corrected for the iR drop in a straightforward manner but face the challenge of a more or less pronounced time dependence in the recorded current or potential. Hence in the current work, we choose to average the currents recorded in a set time interval, see experimental section.

On the other hand, apart from these systematic differences which should lead to a constant shift in activity between all catalysts, the different measurement results of the 50.6 wt. % catalyst in Figure 6 indicate that an automized and standardized procedure might not always be suitable to ensure that each catalyst exhibits its optimal, intrinsic performance. For example, an improved cleaning procedure in oxygen might improve the performance (in the specific case shown here, in the RDE measurements) while for other catalysts it might lead to slight degradation, e.g., in case of small particles. Furthermore, the SEM-EDS cross sections demonstrate substantially different thicknesses of the Pt/C catalyst films depending on the Pt loading on the carbon support.

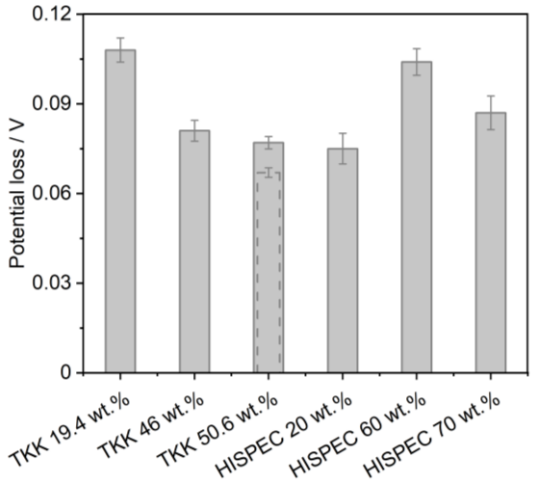

Figure 6: Comparison of the corresponding potential at a current of 5 A m_{Pt}^{-2} from RDE and GDE. The potential loss is a result of subtraction between the averaged corresponding potential in RDE and GDE. The bar from TKK 50.6 wt.% Pt/C with the dashed edge is a measurement result with cleaning the catalyst surface in Ar saturated electrolyte in RDE, while the same catalyst with a bar of solid edge is a measurement result companied with an optimized cleaning procedure (O_2 saturated electrolyte). The given error is the standard deviation for the difference in averaged corresponding potential at the current of 5 A m_{Pt}^{-2} between RDE and GDE.

Furthermore, the activity difference in RDE and GDE can be in part be attributed to the same, unoptimized ink composition for all Pt/C catalysts. For example, a fixed carbon to Nafion (C:N) mass ratio, might not be the best recipe for all the different catalysts. The different Pt loadings on the carbon support, the different Pt particle size distributions as well as different carbon supports might require specific ink compositions for every single catalyst to optimize the performance in the GDE setup; knowledge that is commonly known for MEA measurements and is part of the optimization of fuel cell catalyst layers. [36]

3.4.3 Catalyst layer optimization

To investigate this hypothesis, we analyzed the specific ORR activity (SA) of a moderately performing catalyst, i.e., the HISPEC 70 wt. % at different C:N mass ratios. As demonstrated in Figure 7, the conventional ink recipe (C:N=1:1) does not lead to the best performance of the HISPEC 70 wt. % catalyst. The obtained maximum power density strongly depends on the C:N ratio in the ink (Figure 7). By changing the C:N ratio, the maximum power density can be almost doubled from about 0.4 W cm^{-2} to about 0.7 W cm^{-2}. A standardized ink recipe therefore leads to an “underperformance” of certain catalysts. For a meaningful comparison of different catalysts in a GDE, it is therefore important to consider optimizing the ink composition for every single catalyst.

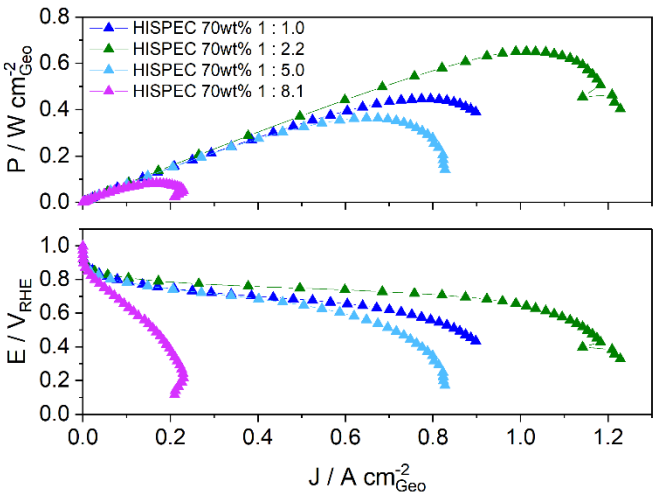

Figure 7: Comparison of different carbon to Nafion ratios (C:N) of HISPEC 70wt%. The power density of HISPEC 70wt% strongly depends on the amount of Nafion added to the ink. The standard procedure suggests a C:N ratio of 1:1. However, measurements made with the GDE setup show higher power density for a C:N ratio of 1:2.2. By adding significantly more Nafion, the power density drops down.

To demonstrate this conclusion even further, and to analyze which characteristics are crucial for a good performance of a specific Pt/C catalyst, we also analyzed the influence of the Pt to Nafion (Pt:N) ratio of this specific catalyst by introducing additional carbon support in the catalyst ink. In the plot in Figure 8 it is demonstrated that at 0.9 V_{RHE} the ORR performance increases with increasing C:N ratio. With regards to the Pt:N ratio, it seems that the ORR performance increases with increasing ratio as well. However, this behavior changes as soon as higher current densities are reached. At 0.8 V_{RHE} the highest ORR current density was reached with a Pt:N ratio of 1 instead of a ratio more than 2 at 0.9 V_{RHE}. Furthermore, it is shown that at this Pt:N ratio, the C:N ratio does not have a substantial influence on the current density anymore. This trend gets even more pronounced at 0.7 V_{RHE}. The highest current density for the HISPEC 70 wt. % catalyst were obtained with a Pt:N ratio of 1 (by adding carbon support to the ink) *and* a C:N ratio of 1.

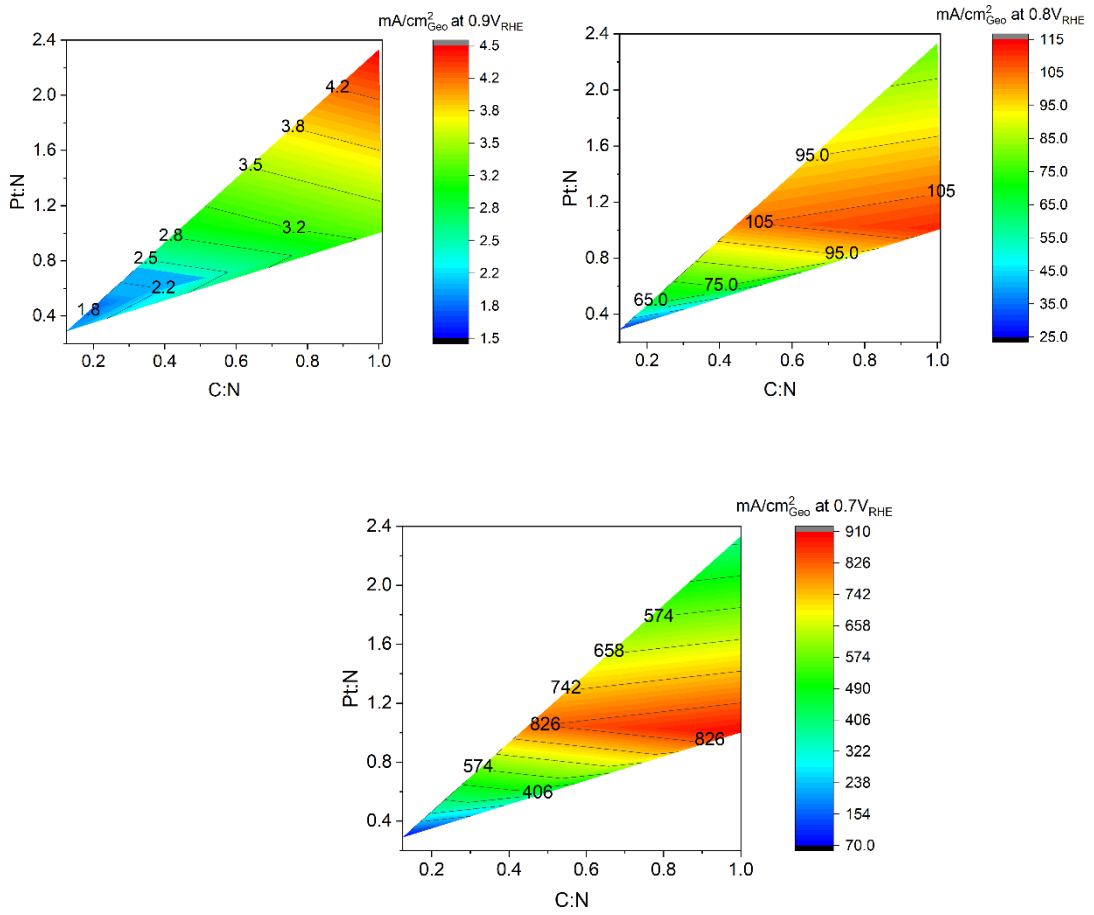

Figure 8: Comparison of the influence of Pt:N and C:N ratios on ORR activities of HISPEC 70wt% at 0.9V_{RHE}, 0.8V_{RHE} and 0.7V_{RHE}. At 0.9V both Pt:N and C:N ratio determine the obtained current density of HISPEC 70wt%. A high Pt:N ratio and a C:N ratio around 1 gave the highest current densities. However, at lower voltages the Pt:N ratio becomes the key ratio. There is a clear trend towards a Pt:N ratio of 1. The ORR activities are averaged values of 3 measurements.

Catalyst	Pt NP size (nm)		Theoretical M-ECSA ($m^2\ g_{Pt}^{-1}$)	M-ECSA ($m^2\ g_{Pt}^{-1}$)		MA ($A\ g_{Pt}^{-1}$)			SA ($A\ m_{Pt}^{-2}$)			
	TEM	SAXS	Based on TEM	RDE	GDE	RDE (0.9 V)	GDE (0.9 V)	GDE (0.8 V)	RDE (0.9 $V_{Pos.}$)	RDE (0.9 $V_{Neg.}$)	GDE (0.9 V)	GDE (0.8 V)
TKK 19.4 wt.%	1.6 ± 0.4	1.9 ± 0.3	175	151.3 ± 7.5	120.1 ± 2.3	163.4 ± 59	12.2 ± 0.6	330	3.37 ± 0.49	1.08 ± 0.39	0.1	2.75
TKK 46 wt.%	2.9 ± 0.8	2.8 ± 0.5	96.5	90.3 ± 1.1	84.6 ± 5	108.4 ± 11.8	26.7 ± 0.9	660	5.84 ± 0.99	1.20 ± 0.13	0.3	7.8
TKK 50.6 wt.%	4.7 ± 1.1	5.4 ± 1.7	59.5	61.4 ± 3.3	49 ± 0.2	55.3 ± 7.4	16.8 ± 0.4	364	3.18 ± 0.28 4.20 ± 0.36	0.90 ± 0.11 1.68 ± 0.14	0.3	7.43

HISPEC 20 wt.%	2.9 ± 0.8	3.3 ± 1.1	96.5	91.8 ± 2.1	57.8 ± 3.2	175.3 ± 8.3	19.4 ± 2.7	517	5.64 ± 1.21	1.91 ± 0.09	0.3	8.95
HISPEC 60 wt.%	2.9 ± 1	3.3 ± 0.8	96.5	86.5 ± 3.4	57 ± 2	174.7 ± 17.3	9.7 ± 0.1	280	5.69 ± 1.14	2.02 ± 0.20	0.2	5
HISPEC 70 wt.%	3.5 ± 1.5	4 ± 0.8	79.8	61.5 ± 0.7	45.3 ± 1.6	113.2 ± 40	21.4 ± 0.7	379	6.77 ± 2.00	1.84 ± 0.65	0.5	8.4

Table 1: The font in red from TKK 50.6 wt.% is the result with potential cycling in O_2 for catalyst surface cleaning. In addition, the SA results from positive direction are based on calculation including all measurement results (5 or 6, without cutting down the highest and lowest value), but the SA results from negative are with cutting down the highest and lowest value to get the average value, since I calculate the biggest difference between with and w o the highest and lowest value is 7%, so I did not add the values without cutting down … from negative in this table, also because the space is too limited.

4 Conclusion

In the presented work, the ORR performance of six commercial Pt/C catalyst is compared in a GDE setup. As benchmark, the same catalysts are compared in RDE measurements according to standardized procedures that are assumed to showcase the *intrinsic* ORR activity of the respective catalysts. The work clearly demonstrates the challenges but also the strengths of the GDE approach. In the last ten years several RDE studies demonstrated, the importance of the film quality for obtaining the intrinsic ORR activity of a catalyst, research work that is still ongoing [37]. At the same time the popularity of the RDE approach is at least partially owed to its simplicity and the availability of all required instruments. The presented GDE measurements indicate that the influence of the film quality on the obtained results in this approach is at least equally important as in the RDE approach. However, to find broad application, a simple and straight-forward film preparation method should be applied such as the vacuum filtration technique that only requires standard equipment that is available in most research laboratories and leads to reproducible results in film quality. Most likely, as for the RDE approach, further work on

establishing standardized procedures and the use of benchmarks will be essential to obtain meaningful results.

On the other hand, the results clearly demonstrate the potential of the GDE approach to bridge RDE and MEA measurements thus helping to commercialize new ORR catalysts. Most importantly, the GDE approach allows focusing on relevant current densities that are inaccessible in RDE measurements. Moreover, the optimization of characteristics such as the ink recipe or the applied catalyst loading on the GDL for each individual catalyst is feasible in a much simpler manner than in elaborate MEA testing. Therefore, the GDE approach has the clear potential to reach similar popularity as the RDE approach.

Acknowledgments

This work was supported by the Swiss National Science Foundation (SNSF) via the project No. 200021_184742. Jia Du acknowledges funding from the China Scholarship Council (CSC). Jonathan Quinson acknowledges the European Union's Horizon 2020 research and innovation program under the Marie Skłodowska-Curie grant agreement No. 840523 (CoSolCat). S. B. Simonsen and L. Theil Kuhn, Technical University of Denmark, are thanked for access to TEM. The Niels Bohr Institute, University of Copenhagen, for access to SAXS equipment and in particular J. J. K. Kirkensgaard.

References

[1] "Paris climate agreement." https://unfccc.int/process-and-meetings/the-paris-agreement/the-paris-agreement.

[2] IPCC, "Global Warming of 1.5°C. An IPCC Special Report on the impacts of global warming of 1.5°C above pre-industrial levels and related global greenhouse gas emission pathways, in the context of strengthening the global response to the threat of climate change," 2018.

[3] S. E. Hosseini and M. A. Wahid, "Hydrogen production from renewable and sustainable energy resources: Promising green energy carrier for clean development," *Renew. Sustain. Energy Rev.*, vol. 57, pp. 850–866, 2016, doi: 10.1016/j.rser.2015.12.112.

[4] L. Carrette, K. A. Friedrich, and U. Stimming, "Fuel Cells - Fundamentals and Applications," *Fuel Cells*, vol. 1, no. 1, pp. 5–39, 2001, doi: 10.1002/1615-6854(200105)1:1<5::aid-fuce5>3.0.co;2-g.

[5] O. Gröger, H. A. Gasteiger, and J.-P. Suchsland, "Review—Electromobility: Batteries or Fuel Cells?," *J. Electrochem. Soc.*, vol. 162, no. 14, pp. A2605–A2622, 2015, doi: 10.1149/2.0211514jes.

[6] K. Shinozaki, J. W. Zack, R. M. Richards, B. S. Pivovar, and S. S. Kocha, "Oxygen reduction reaction measurements on platinum electrocatalysts utilizing rotating disk electrode technique: I. Impact of impurities, measurement protocols and applied corrections," *J. Electrochem. Soc.*, 2015, doi: 10.1149/2.1071509jes.

[7] D. Siegmund *et al.*, "Crossing the Valley of Death: From Fundamental to Applied Research in Electrolysis," *JACS Au*, vol. 1, no. 5, pp. 527–535, 2021, doi: 10.1021/jacsau.1c00092.

[8] B. Han *et al.*, "Record activity and stability of dealloyed bimetallic catalysts for proton exchange membrane fuel cells," *Energy Environ. Sci.*, vol. 8, no. 1, pp. 258–266, Dec. 2015, doi: 10.1039/c4ee02144d.

[9] T. Yoshizumi, H. Kubo, and M. Okumura, "Development of High-Performance FC Stack for the New MIRAI," *SAE Int.*, 2021, doi: 10.4271/2021-01-0740.

[10] G. K. H. Wiberg, M. Fleige, and M. Arenz, "Gas diffusion electrode setup for catalyst testing in concentrated phosphoric acid at elevated temperatures," *Rev. Sci. Instrum.*, vol. 86, no. 2, 2015, doi: 10.1063/1.4908169.

[11] M. Inaba, A. W. Jensen, G. W. Sievers, M. Escudero-Escribano, A. Zana, and M. Arenz, "Benchmarking high surface area electrocatalysts in a gas diffusion electrode: Measurement of oxygen reduction activities under realistic conditions," *Energy Environ. Sci.*, vol. 11, no. 4, 2018, doi: 10.1039/c8ee00019k.

[12] C. Zalitis, A. Kucernak, X. Lin, and J. Sharman, "Electrochemical Measurement of Intrinsic Oxygen Reduction Reaction Activity at High Current Densities as a Function of Particle Size for Pt4- xCox/C (x = 0, 1, 3) Catalysts," *ACS Catal.*, vol. 10, no. 7, pp. 4361–4376, 2020, doi:

10.1021/acscatal.9b04750.

[13] C. M. Zalitis, D. Kramer, and A. R. Kucernak, “Electrocatalytic performance of fuel cell reactions at low catalyst loading and high mass transport,” *Phys. Chem. Chem. Phys.*, 2013, doi: 10.1039/c3cp44431g.

[14] L. Pan, S. Ott, F. Dionigi, and P. Strasser, “Current challenges related to the deployment of shape-controlled Pt alloy oxygen reduction reaction nanocatalysts into low Pt-loaded cathode layers of proton exchange membrane fuel cells,” *Curr. Opin. Electrochem.*, vol. 18, no. October, pp. 61–71, 2019, doi: 10.1016/j.coelec.2019.10.011.

[15] K. Ehelebe, D. Seeberger, M. T. Y. Paul, S. Thiele, K. J. J. Mayrhofer, and S. Cherevko, “Evaluating Electrocatalysts at Relevant Currents in a Half-Cell: The Impact of Pt Loading on Oxygen Reduction Reaction,” *J. Electrochem. Soc.*, vol. 166, no. 16, pp. F1259–F1268, 2019, doi: 10.1149/2.0911915jes.

[16] B. A. Pinaud, A. Bonakdarpour, L. Daniel, J. Sharman, and D. P. Wilkinson, “Key Considerations for High Current Fuel Cell Catalyst Testing in an Electrochemical Half-Cell,” *J. Electrochem. Soc.*, 2017, doi: 10.1149/2.0891704jes.

[17] S. Alinejad *et al.*, “Testing fuel cell catalysts under more realistic reaction conditions: accelerated stress tests in a gas diffusion electrode setup,” *J. Phys. Energy*, vol. 2, no. 2, p. 024003, Jan. 2020, doi: 10.1088/2515-7655/ab67e2.

[18] J. Schröder *et al.*, “The Gas Diffusion Electrode Setup as Straightforward Testing Device for Proton Exchange Membrane Water Electrolyzer Catalysts,” *JACS Au*, vol. 1, no. 3, pp. 247–251, Feb. 2021, doi: 10.1021/jacsau.1c00015.

[19] J. Schröder *et al.*, “A New Approach to Probe the Degradation of Fuel Cell Catalysts under Realistic Conditions: Combining Tests in a Gas Diffusion Electrode Setup with Small Angle X-ray Scattering,” *J. Electrochem. Soc.*, 2020, doi: 10.1149/1945-7111/abbdd2.

[20] M. Inaba, J. Quinson, and M. Arenz, “pH matters: The influence of the catalyst ink on the oxygen reduction activity determined in thin film rotating disk electrode measurements,” *J. Power Sources*, vol. 353, pp. 19–27, 2017, doi: 10.1016/j.jpowsour.2017.03.140.

[21] J. Du, J. Quinson, D. Zhang, F. Bizzotto, A. Zana, and M. Arenz, “Bifunctional Pt-IrO_2 Catalysts for the Oxygen Evolution and Oxygen Reduction Reactions: Alloy Nanoparticles versus Nanocomposite Catalysts,” *ACS Catal.*, vol. 11, no. 2, pp. 820–828, doi: 10.1021/acscatal.0c03867.

[22] J. Du, J. Quinson, A. Zana, and M. Arenz, “Elucidating Pt-Based Nanocomposite Catalysts for the Oxygen Reduction Reaction in Rotating Disk Electrode and Gas Diffusion Electrode Measurements,” *ACS Catal.*, vol. 11, no. 12, pp. 7584–7594, doi: 10.1021/acscatal.1c01496.

[23] K. J. J. Mayrhofer, D. Strmcnik, B. B. Blizanac, V. Stamenkovic, M. Arenz, and N. M. Markovic, “Measurement of oxygen reduction activities via the rotating disc electrode method: From Pt model surfaces to carbon-supported high surface area catalysts,” *Electrochim. Acta*, vol. 53, no. 7, pp. 3181–3188, 2008, doi:

10.1016/j.electacta.2007.11.057.

[24] M. Inaba, J. Quinson, J. R. Bucher, and M. Arenz, “On the preparation and testing of fuel cell catalysts using the thin film rotating disk electrode method,” *J. Vis. Exp.*, vol. 2018, no. 133, 2018, doi: 10.3791/57105.

[25] D. Zhang, J. Du, J. Quinson, and M. Arenz, “On the electro-oxidation of small organic molecules: towards a fuel cell catalyst testing platform with realistic reaction environment,” *ChemRxiv. Prepr.*, 2021, doi: 10.33774/chemrxiv-2021-j5vb5.

[26] G. S. Harzer, J. N. Schwämmlein, A. M. Damjanović, S. Ghosh, and H. A. Gasteiger, “Cathode Loading Impact on Voltage Cycling Induced PEMFC Degradation: A Voltage Loss Analysis,” *J. Electrochem. Soc.*, vol. 165, no. 6, pp. F3118–F3131, 2018, doi: 10.1149/2.0161806jes.

[27] A. J. Bard and L. R. Faulkner, *Electrochemical Methods: Fundamentals and Applications*, 2nd Editio. Wiley-VCH Verlag.

[28] U. A. Paulus, T. J. Schmidt, H. A. Gasteiger, and R. J. Behm, “Oxygen reduction on a high-surface area Pt / Vulcan carbon catalyst : A thin-film rotating ring-disk electrode study Oxygen reduction on a high-surface area Pt / Vulcan carbon catalyst : a thin-film rotating ring-disk electrode study,” *Res. gate*, vol. 495, no. January 2001, pp. 134–145, 2014, doi: 10.1016/S0022-0728(00)00407-1.

[29] M. Nesselberger, S. Ashton, J. C. Meier, I. Katsounaros, K. J. J. Mayrhofer, and M. Arenz, “The particle size effect on the oxygen reduction reaction activity of Pt catalysts: Influence of electrolyte and relation to single crystal models,” *J. Am. Chem. Soc.*, vol. 133, no. 43, 2011, doi: 10.1021/ja207016u.

[30] K. Kodama *et al.*, “Catalyst Poisoning Property of Sulfonimide Acid Ionomer on Pt (111) Surface,” *J. Electrochem. Soc.*, vol. 161, no. 5, pp. F649–F652, Mar. 2014, doi: 10.1149/2.051405jes.

[31] H. A. Gasteiger, S. S. Kocha, B. Sompalli, and F. T. Wagner, “Activity benchmarks and requirements for Pt, Pt-alloy, and non-Pt oxygen reduction catalysts for PEMFCs,” *Applied Catalysis B: Environmental*. pp. 9–35, 2005, doi: 10.1016/j.apcatb.2004.06.021.

[32] S. S. Kocha *et al.*, “Best Practices and Testing Protocols for Benchmarking ORR Activities of Fuel Cell Electrocatalysts Using Rotating Disk Electrode,” *Electrocatalysis*, vol. 8, no. 4, pp. 366–374, Jul. 2017, doi: 10.1007/s12678-017-0378-6.

[33] D. Voiry *et al.*, “Best Practices for Reporting Electrocatalytic Performance of Nanomaterials,” *ACS Nano*, vol. 12, no. 10, pp. 9635–9638, 2018, doi: 10.1021/acsnano.8b07700.

[34] V. Yarlagadda, S. E. McKinney, C. L. Keary, L. Thompson, B. Zulevi, and A. Kongkanand, “Preparation of PEMFC Electrodes from Milligram-Amounts of Catalyst Powder,” *J. Electrochem. Soc.*, vol. 164, no. 7, pp. F845–F849, Jun. 2017, doi: 10.1149/2.1461707jes.

[35] N. M. Markovíc and P. N. Ross, “Surface science studies of model fuel cell electrocatalysts,”

Surf. Sci. Rep., vol. 45, no. 4–6, pp. 117–229, 2002, doi: 10.1016/s0167-5729(01)00022-x.

[36] T. Yoshizumi, H. Kubo, and M. Okumura, "Development of High-Performance FC Stack for the New MIRAI," 2021, doi: https://doi.org/10.4271/2021-01-0740.

[37] M. Inaba, Y. Kamitaka, and K. Kodama, "Eliminating the need for craftsmanship: Facile and precise determination of oxygen reduction reaction activity by spraying catalyst ink on rotating disk electrode," *J. Electroanal. Chem.*, vol. 886, no. December 2020, p. 115115, 2021, doi: 10.1016/j.jelechem.2021.115115.

Supporting information

Details SAXS analysis and results

The average volume of nanoparticle from population 1 and from population 2, $<V>_1$ and $<V>_2$ respectively, lead to define volume fraction of population 1, Φ_{V1}, and volume fraction of population 2, Φ_{V2}, as:

$$\Phi_{V1} = \frac{N_1 < V >_1}{N_1 < V >_1 + N_2 < V >_2} = 1 - \Phi_{V2}$$

$$\frac{\Phi_{V1}}{\Phi_{V2}} = \frac{N_1 < V >_1}{N_2 < V >_2}$$

$$\frac{N_1}{N_2} = \frac{\Phi_{V1} < V >_2}{\Phi_{V2} < V >_1}$$

where N_1 and N_2 are the number of nanoparticles in the population 1 or 2 respectively.

From the SAXS data acquisition we have the relationship between the retrieved coefficient C_1 and C_2 given by $C_i = k.\ \Phi_{vi}.\ <V>_i$ where i=1 or 2 and k is a constant.

$$k = \frac{C_1}{\Phi_{V1} < V >_1} = \frac{C_2}{\Phi_{V2} < V >_2} = \frac{C_2}{(1 - \Phi_{V1}) < V >_2}$$

$$\frac{\Phi_{V1}}{1 - \Phi_{V1}} = \frac{C_1 < V >_2}{C_2 < V >_1}$$

$$\Phi_{V1} = \frac{1}{1 + \frac{C_2 < V >_1}{C_1 < V >_2}}$$

In order to weight the probability density function by the area or surface fractions we consider $<A>_1$ and $<A>_2$ as the average area of the nanoparticles from population 1 and 2, respectively:

$$\Phi_{A1} = \frac{N_1 < A >_1}{N_1 < A >_1 + N_2 < A >_2} = 1 - \Phi_{A2} = \frac{1}{1 + \frac{N_2 < A >_2}{N_1 < A >_1}}$$

$$\Phi_{A1} = \frac{1}{1 + \frac{\Phi_{V2} < V >_1 < A >_2}{\Phi_{V1} < V >_2 < A >_1}}$$

$$\Phi_{A1} = \frac{1}{1 + \frac{C_2 (< V >_1)^2 < A >_2}{C_1 (< V >_2)^2 < A >_1}}$$

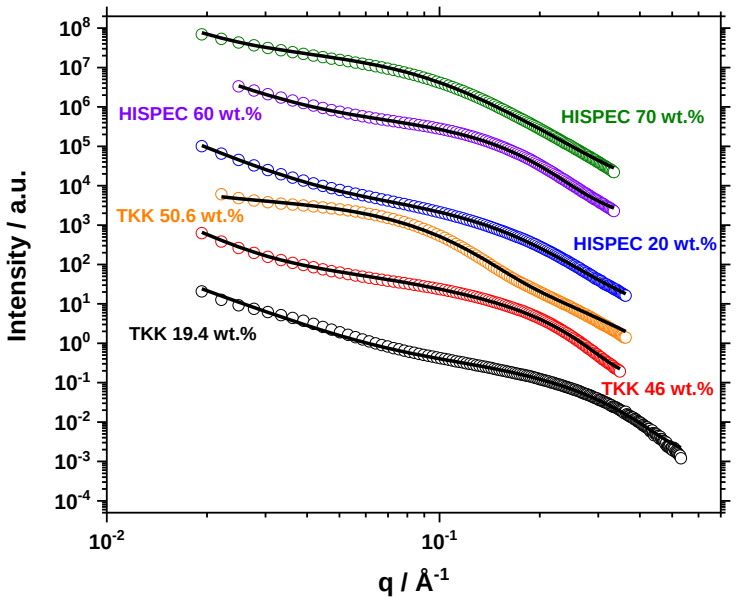

Figure S 1: Background subtracted SAXS data and the related fits for the different samples, as indicated.

Table S 1 SAXS fitting parameters for fits corresponding to *Figure S 1*.

Sample	A*10⁶	n	R₁ (Å)	σ₁	C₁	R₂ (Å)	σ₂	C₂	d / nm [a]	σ / nm [b]
TKK 19.4 wt.%	115	3.1	8.6	0.12	0.002	10.1	0.3	0.005	1.9	0.3
TKK 46 wt.%	8	4.0	13.0	0.20	0.025	20.0	0.4	0.018	2.8	0.5
TKK 50.6 wt.%	40	3.3	26.0	0.30	0.110	-	-	-	5.4	1.7

HISPEC 20 wt.%	100	3.5	15.5	0.33	0.030	-	-	-	3.3	1.1
HISPEC 60 wt.%	150	3.3	16.0	0.25	0.038	-	-	-	3.3	0.8
HISPEC 70 wt.%	52	3.5	15.0	0.25	0.015	25.0	0.3	0.063	4.0	0.8

(a) evaluated as $0.2\ \varphi_{A1}\ e^{\left(\ln(R_1)+\frac{{\sigma_1}^2}{2}\right)} + \ 0.2\ \varphi_{A2}\ e^{(\ln(R_2)+\frac{{\sigma_2}^2}{2})}$

(b) evaluated $0.2\sqrt{{\varphi_{A1}}^2\ [(e^{{\sigma_1}^2}-1).\ e^{(2.\ln(R_1)+{\sigma_1}^2)} + \ {\varphi_{A2}}^2\ [(e^{{\sigma_2}^2}-1).\ e^{(2.\ln(R_2)+{\sigma_2}^2)}}$

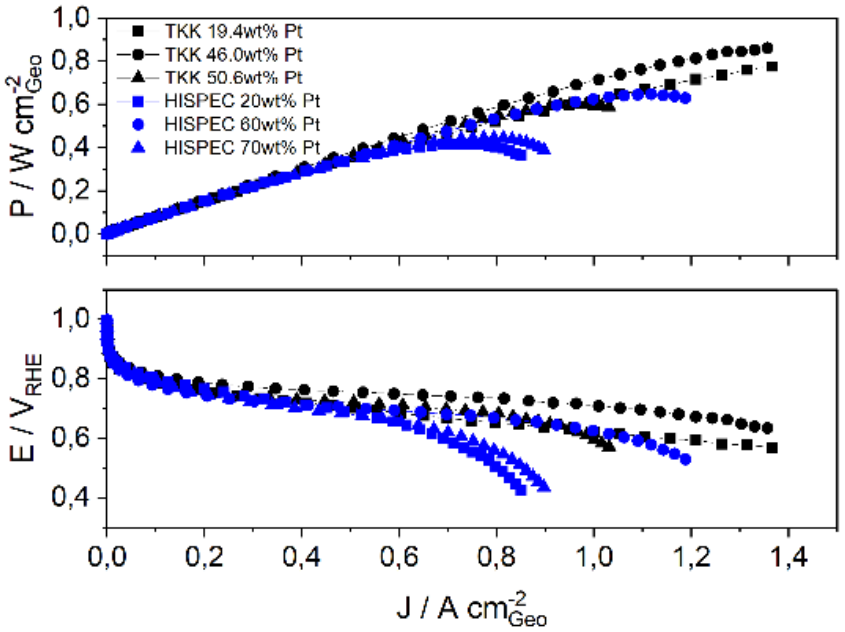

Figure S 2: Comparison of the performance of all investigated catalysts in a GDE setup. The red lines represent catalysts manufactured by Tanaka Kikinzoku Kogyo K.K, the blue lines represent catalysts manufactured by Alfa Aesar. The figure shows the averaged power density of at least three measurements of the same catalyst.

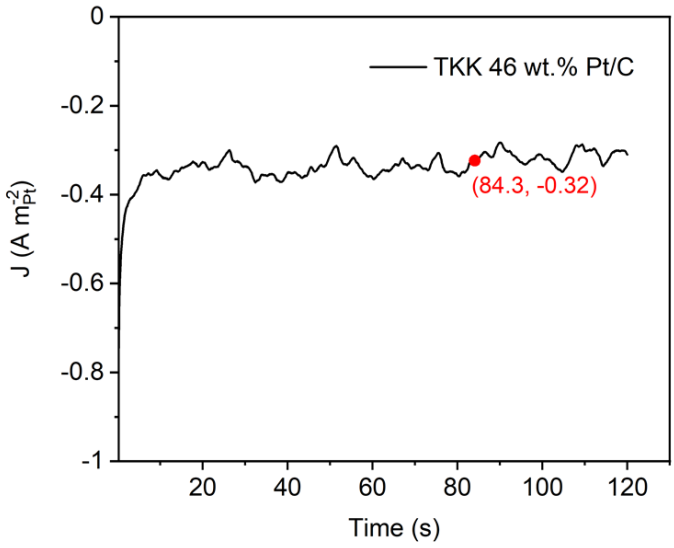

Figure S 3: ORR activity determination under steady state. Potential sweeping was conducted for several cycles with different rotation speed in O2 saturated 0.1 M HClO4, followed by potential jumping to 0.9 VRHE and holding for 2 min. The corresponding current was recorded and normalized by Pt ECSA